Molecular dynamics simulations for hydrogen adsorption at low energy collisions with carbon and boron-nitride nanotubes

F. J. Domínguez-Gutiérrez,[1, a)] C. Martínez-Flores,[2] and R. Cabrera-Trujillo[2]

[1)] *Max-Planck-Institute for Plasma Physics, Boltzmannstrasse 2, 85748 Garching, Germany*

[2)] *Instituto de Ciencias Físicas, Universidad Nacional Autónoma de México, Ap. Postal 43-8, Cuernavaca, Morelos, 62251, México*

(Dated: 4 April 2019)

The capability of carbon (CNT) and boron-nitride (BNNT) nanotubes to absorb hydrogen atoms might indicate if these materials can be used to develop an efficient and fast hydrogen nanosensor device. In this work, we carry out a theoretical study of the hydrogen adsorption mechanism by carbon and boron-nitride nanotubes irradiated by atomic hydrogen in the impact energy range of $0.25 - 100$ eV. Hydrogen adsorption, reflection, and transmission probabilities are reported. The collision dynamics is calculated by performing quantum-classical molecular dynamics (QCMD) simulations within the self-consistent-charge density-functional tight-binding (SCC-DFTB) method. We include fitting curves for the angular distribution of reflected and transmitted H atoms by using a modified Yamamura formula. Results for CNT follows a cosine-like law, while the majority of the projectiles tend to be scattered at angles lower than 60^o for BNNT. Based on previous studies for spherical and planar carbon-based configurations, we analyse the effect of the system's curvature on the hydrogen capture on CNT. We find that for collision energies below 5 eV, the scattering process depends on the carbon system curvature, meanwhile the adsorption is independent for collision energies below 0.5 eV Our results for the hydrogen adsorption rates for both nanotubes suggests that these materials can be used in hydrogen detector devices in a wide impact energy range.

Keywords: Hydrogen detector, QCMD, carbon nanotubes, boron-nitride nanotubes

[a)] Electronic mail: javier.dominguez@ipp.mpg.de

I. INTRODUCTION

In recent years an interest has risen on the study of nanotubular forms of materials as a consequence of the synthesis, properties, and attempts for industrial applications of these nanomaterials. Carbon nanotubes (CNT) form is intermediate between graphite and fullerenes. However, many of the nanotube properties are drastically different from the other forms of carbon. CNTs have applications in a great number of areas such as additives to polymers and catalysts, in autoelectron emission for cathode rays of lighting components, flat displays, gas discharge tubes, telecommunication networks, absorption and screening of electromagnetic waves, energy conversion, lithium battery anodes, hydrogen storage, composite materials (fillers or coatings), nanoprobes, sensors, supercapacitors and many more[1]. The great variety of unconventional mechanical, electrical, and magnetic properties of nanotubes make them important in nanoelectronics. As a nanotube is a surface structure that has been rolled, its whole weight is concentrated in its surface layers. This feature is the origin of the uniquely large unit surface of tubulenes, which in turn predetermines its electrochemical and adsorption properties[2]. The high sensitivity of the electronic properties of nanotubes due to the absorbtion of atoms or molecules on its surface makes CNTs a promising material for the development of superminiaturized chemical and biological sensors[2,3]. The principle operation of these sensors is based on changes in the voltagecurrent ($V - I$) curves of nanotubes as a result of adsorption of specific atoms or molecules on the CNT surface. The use of CNT in sensor devices is one of their most promising applications in electronics with further applications in optoelectronic nano-devices, hydrogen accumulators, electrically insulating, to mention a few[4? –10]. Another application is the development of sensitive and accurate hydrogen detectors, energy carriers, and as chemical reactants[11–14]. Numerous experimental and theoretical efforts have been focused in understanding the electronic properties of CNTs[15–17] and the boron nitride nanotubes (BNNTs)[18–20]. Thus, single-walled carbon nanotubes have been proposed to develop a novel highly sensitive gas sensor[12]. This device is able to operate at room temperature with a sensitivity of 10^3, which provides a step-forward into chemical nanosensors[21]. A fast and low-cost hydrogen sensor has been fabricated by using Pd as catalytic so that the response of this device reaches a 0.01-1% H concentration[14].

A pristine BNNT presents adequate electronic properties to detect hydroperoxyl radical (HO_2) and can be considered as a promising material to develop a sensor device[22]. Also,

doped BNNT is energetically favorable[23] and it seems to be a good choice to detect noble gases, e.g., by the adsorption of He, Ne, Ar, and Kr. A theoretical study of physisorption and chemisorption of H_2 by these systems has demonstrated that a CNT is a better option for a molecular hydrogen sensor than a BNNT one[24]. Therefore, it is of interest to investigate the atomic hydrogen adsorption mechanism of these materials in this work and to search for the advantages and disadvantages to each other. Here, we are mainly focused on the study and understanding of the atomic hydrogen adsorption mechanism of H irradiation on CNT and its comparison with BNNT, where only the physical adsorption process is considered. Furthermore, our results could provide an understanding to develop an optimal gas nanosensor based on these structures.

To the author's knowledge, the majority of the theoretical works have been done based on a direct use of Density Functional Theory (DFT), which for nanotube systems is an expensive computational approach. In our work, we use the self-consistent-charge density-functional tight-binding (SCC-DFTB) method[25,26], which is computationally faster than the traditional DFT approach, to perform numerical simulation of hydrogen atoms when impinging on CNT and BNNT at low collision energies (0.25-100 eV). Our results report the calculation of the adsorption, capture, and scattering rates as a function of the impact energy.

This paper is organized as follows: In section II, we describe the computational method used in this paper. In order to gain a physical insight on our SCC-DFTB results, we compute the potential energy curves of the interaction of a hydrogen atom with the nanotubes, carried out with the same SCC-DFT method, as well as a comparison with a more elaborated DFT approach, as implemented in the Quantum Espresso code. In Section III, we present the results of atomic hydrogen irradiation on the carbon and boron-nitride nanotubes. Finally, in section IV, we give our concluding remarks.

II. COMPUTATIONAL METHOD

The self-consistent charge density-functional tight-binding (SCC-DFTB) method only considers the valence electron interactions in the calculations[25,26]. The total valence electronic densities and energies are obtained by solving numerically the Kohn-Sham (KS) equations by using predetermined tabulated Hamiltonian matrix elements as well as overlap and

repulsive integrals represented by splines that are incorporated into the Slater-Koster parameters Files (SKF)[25,27]. Therefore, the electronic energies are computed as a sum over the occupied single-particle and diatomic repulsive energy contributions. Here, we utilize the SKF pair potentials set for materials science simulations (MATSCI-03)[26], as implemented in the DFTB+ code, version 1.2[28], which shows a good agreement with potential energy curves obtained from more elaborated DFT calculations[29–32]. This demonstrates that the SCC-DFTB results have an accuracy close to those obtained by DFT, but with a smaller computational cost. Since, the DFTB method excludes van der Waals interaction, we include dispersion corrections in our calculations by a Lennard-Jones potential U_{ij} to describe the interaction between atoms i and j[33], where the van der Waals distance and the well depth are obtained from the Universal Force Field parameters[34]. This modification to the DFTB method has been applied to carbon based system such as nanotubes and graphene in good agreement with experimental data[33].

A. CNT and BNNT structures

We choose the zig-zag (6,0) carbon and boron-nitride nanotubes, which have been reported as the likely smallest freestanding single wall CNT[35]. A slab of 144 atoms defines our CNT and BNNT nanotubes with a radius of 4.88 Å and 5.0 Å, respectively. Both systems have a length of 24.12 Å and periodicity on the z-axis is set to simulate an infinite nanotube.

The CNT and BNNT are energy optimized previous computer simulations and calculations. The obtained CNT radius of 4.88 Å is in good agreement with the experimental value of 5 Å by Sun et al.[36]. In Fig. 1, we show the optimized geometry of the nanotube structures where the C-C bond length is 1.45 Å for the CNT, in agreement with the reported results of 1.42 Å[37]. Meanwhile, the B-N bond length of 1.49 Å is obtained for the BNNT, as a consequence of the hexagonal shape of the BN rings.

B. Potential energy curves

We compute static calculations for the Potential Energy Curves (PECs) of a H atom and the main adsorbate sites of a nanotube with the SCC-DFTB method by considering an electronic temperature of 1000 K. This provides information about the potential barriers and

wells that the H atoms have to overcome to be captured or scattered by the nanotubes, in the collision dynamics simulations. The comparison to a more elaborated quantum chemistry approach is carried out by a series of adiabatic calculations with the Quantum Espresso package suit[38] which is based on the DFT method. In general, the PECs are calculated as $\Delta E(r) = E_{NT}(r) - E_N - E_H$, where E_{NT} is the total electronic energy of the nanotube and hydrogen atom at a distance r, as measured from the symmetry axis of the nanotube; E_N is the energy of the isolated nanotube; and E_H the energy of the isolated hydrogen atom. All the atomic nuclei are fixed during the energy calculations.

For the DFT computation of the PECs, we consider the adsorbate sites of the hexagon by defining a small slab for the BNNT and CNT structures. The slab contains 48 atoms with a length of 7.08 Å and a radius of 5.0 Å for the BNNT and 4.88 Å for the CNT, which is smaller that the one used in the SCC-DFTB case because of the need of robust computational resources. The calculations for both systems are performed by using the correlation functionals of Perdew-Burke-Ernzerhof (PBE)[39]. A plane-wave basis set is chosen with a kinetic energy cutoff of 43 Ry (585 eV) and 113 Ry (1537 eV) for the wave functions for the CNT and BNNT, respectively, and 170 Ry (2313 eV) for the charge density and potential for both systems. The ionic cores are modeled with projector augmented wave (PAW) potentials[40]. Integration in the first Brillouin zone was performed using the $1 \times 1 \times 4$ points Monkhorst−Pack sampling[41]. The adiabatic energy calculations are obtained by using an optimized geometry where all the atoms are included in the optimization procedure without any geometry or symmetry constraint.

Adiabatic PECs for the CNT and BNNT cases, obtained by SCC-DFTB, are shown in Figs. 2 and 3 as a function of the H atom distancei , respectively. The H atom is placed in

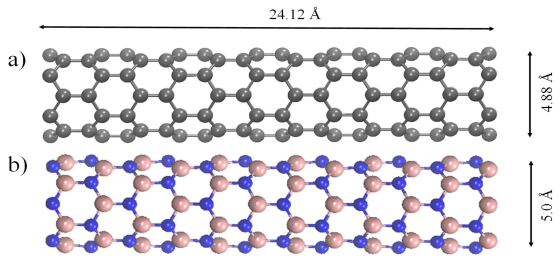

FIG. 1. (Color on-line) Optimized geometries for carbon nanotube in a) and boron-nitride nanotube in b). Carbon atoms in gray, boron in pink, and nitrogen in blue.

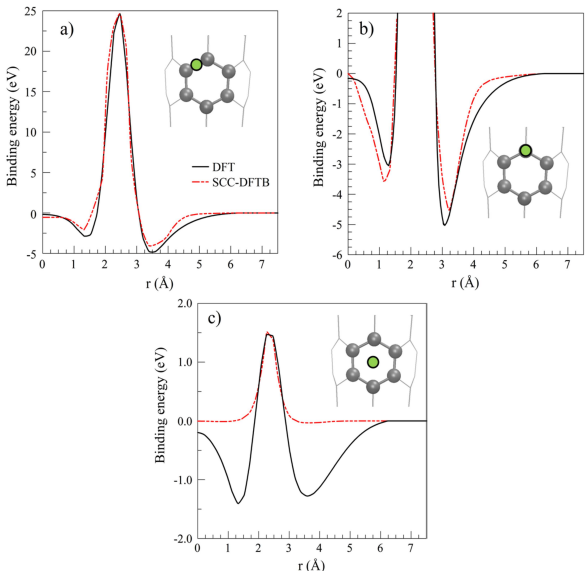

FIG. 2. (Color on-line). Potential energy curves for a hydrogen atom and a CNT, as obtained by DFTBi+ (dashed red line) and DFT-Quantum Espresso (solid red line). We show results for different adsorbate sites of the CNT's hexagon: the bridge in a), above the C atom in b), and the hollow in c). Color pattern: C atoms in gray and H atom in green

straight lines from the center of the nanotube through the different adsorption sites. In Fig. 2, we show the PECs for the interaction of a CNT with a H atom. Considering the three most important adsorbate sites of the hexagonal ring of the CNT: the bridge in Fig. 2a), above the B atom in Fig. 2b), and the hollow in Fig. 2c). There is a good agreement between the results obtained by Quantum Espresso and those by SCC-DFBT for the bridge and above the C atom cases. The potential barrier for the hollow adsorbate site is well reproduced by DFTB, regardless of the discrepancy for the minima points of the PECs. However, this interaction region is almost negligible in our MD simulations due to the impact energy range considered in our work.

For the BNNT case, the PECs are calculated for the following main adsorbate sites: the bridge between the hexagonal rings [Fig. 3a)], the hollow of the hexagon ring [Fig. 3c)], and above the B and N atom [Fig. 3b) and 3d), respectively]. We also compare the obtained PECs by SCC-DFTB (solid lines) to those computed by the Quantum Espresso (dashed lines) for the BNNT. We notice a good agreement between our results for the bridge of the hexagonal rings and above the B and N atoms. Although, the hollow ring adsorbate site presents a discrepancy for the minima of the PECs (wells), the impact energies used in our

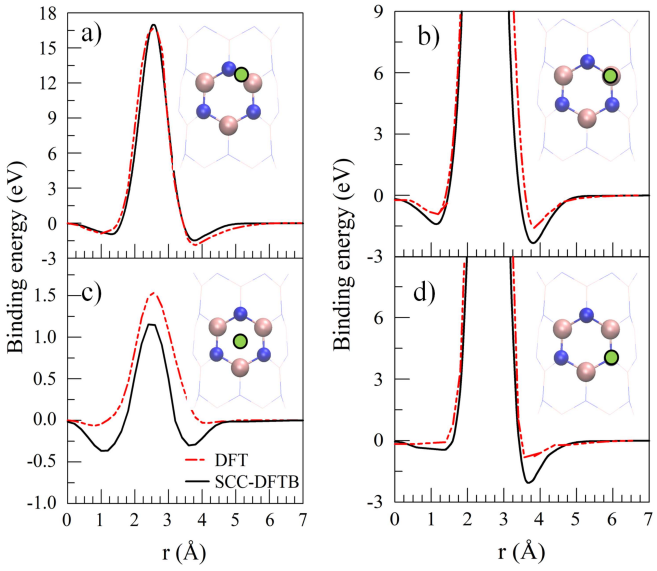

FIG. 3. (Color on-line). The same as in Fig. 2 but for H irradiation on BNNT. We show results for different adsorbate sites of the BNNT's hexagon: the bridge in a), above the B atom in b), the hollow in c), and above the N atom in d). Color pattern: B atoms in pink, N atoms in blue, and H atom in green

QCMD simulations are higher than the difference energy of the wells. Consequently, this discrepancy plays a negligible role in our dynamical calculations.

C. Nanotubes irradiation by atomic hydrogen

We use the DFTB+ code to energy optimize the structures of the nanotubes, followed by a thermalization process at 300 K with a Nosé-Hoover thermostat[30,31]. Then, we use the velocity Verlet algorithm for the collision dynamics with a time step of 0.25 fs. The central part of the nanotubes is bombarded with 2048 H atoms that are homogeneously distributed on a square-shaped target area of 1 nm^2 to take into account all the adsorbate sites of the hexagonal rings of both nanotubes. Each H atom is impinging from a distance of 15 Å measured from the center of the nanotubes with independent trajectories directed towards the same target. This is done to avoid inter-cell hydrogen interactions. We consider the following impact energies: 0.25, 0.5, 1, 2, 5, 8, 10, 20, 30, 50, and 100 eV, with a commensurate velocity given by $v = \sqrt{2E_p/m} = \sqrt{v_x^2 + v_y^2 + v_z^2}$, where E_p is the impact energy and m is the mass of the projectile. The velocity vector of the hydrogen atoms is randomly oriented onto the nanotube to cover all the adsorbate sites. A Fermi-Dirac smearing is utilized

in the MD simulations at an electronic temperature of 1000 K. Lennard-Jones dispersion corrections are included in the calculations to take into account long distance terms in the pair-potentials[33]. Our typical collision dynamics last for 500 fs for impact energies below 10 eV to ensure stability at the end of the dynamics once the target and projectile are separated or bound. At impact energies above 10 eV, the majority of H atoms are reflected or transmitted by the target, which sets the simulation time at 300 fs. The numerical simulations are performed by using the embarrassing parallelization technique within the 160-240 cores of the computer cluster. The probability of reflection, transmission, and adsorption of the events of hydrogen irradiation on the nanotubes for the impact energies of 0.25 to 100 eV is calculated as $(N_H^u)/N_{TH}$, where N_{TH} is the total number of incident hydrogen atoms and N_H^u is the number of scattered ($u = s$) (transmitted or reflected), or internally or externally captured H ($u = c$) atoms, respectively.

III. RESULTS

The results for the probability of adsorption and capture of H atoms in collisions with BNNT and CNT are reported in this section. We also present results for the reflected and transmitted H as a function of the impact energy and deflection angle.

A. Hydrogen scattering and adsorption probabilities

In Fig. 4, we report the calculated probability for a H atom being captured and scattered by the nanotubes as a function of the impact energy. Results for the BNNT are presented in Fig 4a) and for CNT in Fig. 4b). Obtained results at impact energy < 0.5 have to be considered with care due to the need of quantum corrections to the nuclear dynamics. If the impact energy is chosen to be close to the top of the barrier, some contributions from the tunneling effect can occur, which are not taken into account by the classical (over-barrier) approximation of the MD simulation. With this considerations, the probability for binding a H atom outside of the nanotube wall, defined as exo-bond, is dominant at impact energies below 1 eV for both systems. All the H impacts are exo-bound to the BNNT at impact energies below 2 eV, where about 50 % of the H atoms are reflected and the rest are exo-bound to the BNNT wall. There is no H capturing process by the BNNT due to the low

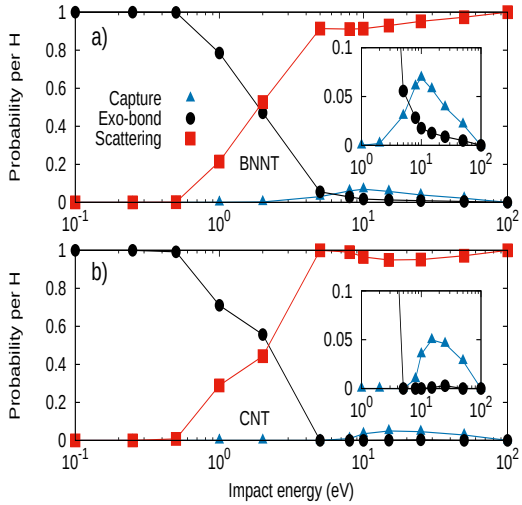

FIG. 4. (Color on-line) Probability of H being captured, exo-bonding, and scattering per H as a function of the impact energy for BNNT in a) and CNT in b). Inset graphs show the probability of H capture and adsorption in the 10-100 eV for better visualization.

impact energy of the projectiles. The percentage of H captured by the BNNT increases for impact energies higher than 2 eV [inset of Fig. 4a)] with a maximum of 7 % at 10 eV. The values for hydrogen capture at 10 and 20 eV are in reasonably good agreement with the theoretical results of Ebrahimi-Nejad et al.[42] with 5.0 % for a (7,7) nanotube. Consequently, more H impacts overcome the PEC barriers of the hexagon hollow and bridge adsorbate sites (Fig. 3) and became retained inside the nanotube.

For the CNT case, Fig. 4b), all H atoms are adsorbed at low impact energies (< 2 eV) similar to the BNNT case. The CNT system has a maximum capturing probability of 5.0 % at 15 eV. A difference between the CNT and BNNT systems is found at 5 eV, where all the H atoms are reflected by the CNT while for the BNNT system about 8 % of the impacts are adsorbed. For the BNNT at 5 eV, 5 % of the H impacts are exo-bond to the wall and approximately 3 % of H atoms are captured inside the nanotube. Another difference between the nanotubes is that the impact energy range for H capture by the BNNT is larger than the one for CNT. Also, it is observed that at 10 eV impact energy the CNT just starts to capture H [inset of Fig. 4b)], in contrast to the BNNT case [inset of Fig. 4a)] where the maximum of the H capture probability occurs.

In previous works, we have studied the probability of atomic H capturing and adsorption for Fullerenes (C_{60})[32] and for graphene by Ehemann et al[30]. Therefore, it is worth comparing

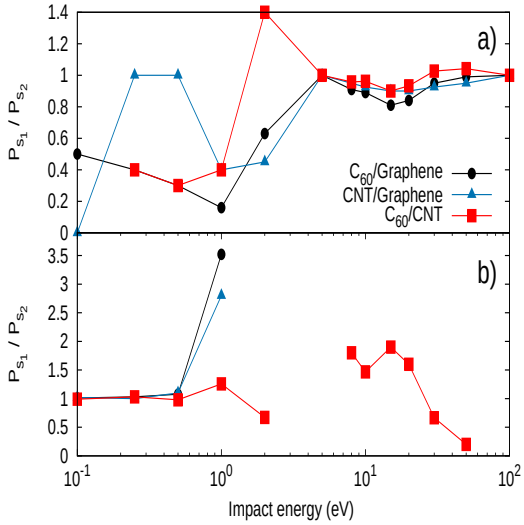

FIG. 5. (Color on-line). Ratio of the probability of scattering in a), and adsorption in b), expressed as P_{S_1}/P_{S_2} for fullerene[31], graphene[30], and CNT as a function of the impact energy. P_S means the probability of scattering or adsorption of each system. The three C-atom arrangement scatter atomic H impact after an impact energy of 5 eV with the same ratio.

these results to investigate the effect of the atomic C arrangement on the H capturing process, since a C_{60} fullerene and a CNT can be built from a graphene sheet[43]. In Fig. 5, we show the ratio of the probability of scattering (transmitted and reflected H impacts) in a), and adsorption (capture and exo-bound) in b) for different systems, which is expressed as P_{S_1}/P_{S_2} with P_S the probability of scattering or adsortion of the system. It is observed, Fig. 5-a), that the three C-atoms geometries scatter about all the H impact at impact energies higher than 5 eV with almost the same ratio. Meanwhile, Fig. 5-b) shows that only CNT and C_{60} systems capture H atoms in the range of 8-50 eV, as expected. These two systems also adsorb more H impacts than a graphene sheet at impact energies around 10 eV. This comparison helps to see the effect of the atomic carbon arrangement in the atomic hydrogen adsorption mechanism.

In Fig. 6, we report all the events of the H atoms captured by the BNNT in a) and CNT in b) at 0.5 eV where all the atoms are exo-bound to the nanotube wall (green $\times$ symbols). In the same figure, we show results at 10 eV for the BNNT and 15 eV for the CNT where the maximum of H capture probability is located (orange + symbols). The left-hand side of the figure shows the horizontal orientation of the nanotubes ($y-z$ axis) to visualize all

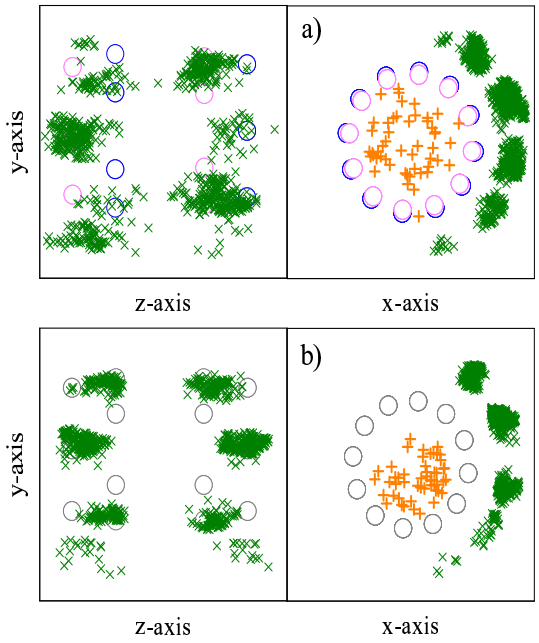

FIG. 6. (Color on-line). Final positions of capturing events for H impact at 0.5 and 10 eV by the BNNT in a) and 0.5 and 15 eV by CNT in b) which show all the independent final trajectories overlapped. Clustering of H atoms are observed around the B and N atoms for the BNNT at 0.5 eV. Note that at this low impact energy, some H atoms are also bound at the bridge adsorbate site. At 10 eV, captured H atoms are gathered around the center of the BNNT, in contrast to the results for the CNT. Colors: Boron and nitrogen are colored in pink and blue, respectively; carbon atoms are in gray; and H final positions are shown by green $\times$ symbols for exo-bonding and orange $+$ symbols for the capture process.

the events after bombarding. We also present the $y-x$ axis view of the nanotubes in the right-hand side of the figure, to show the final position of the H atoms that are captured by the nanotubes.

Fig. 6a) shows the most probable positions of the adsorbed H atoms (green $\times$ symbols) for the BNNT. We note that the formation of H clustering, after overlapping all the independent trajectories, is around the B atoms for a collision energy of 0.5 eV. Other H impacts tend to be bound to the bridge adsorbate site. These results are in agreement with the PEC discussed above and with the results reported by Wu et al[9]. For the atomic H capturing process at 10 eV, the H atoms are gathered around the center of the BNNT. Also, note that some H impacts are bound to the B and N atoms inside the nanotube. In Fig. 6b) the clustering of the H impact is mainly above the C atoms and at the bridge adsorbate sites,

for the collision energy of 0.5 eV, as expected. However, captured H atoms tend to be bound to the C atoms inside the nanotube. A quite similar structure behavior is also reported by Froudakis et al.[44]. These H atoms do not form clusters around the center of the nanotube, as observed in the BNNT system.

We notice that the H impacts are more spread out for the BNNT than for the CNT. For the BNNT case, all the H atoms that are exo-bound cover half of the nanotube and show that the binding mostly occurs where they impinge. However the H impacts tend to cover only the central part of the CNT system. This is due to the different atomic radius for the B (0.85 Å) and N (0.65 Å) atoms[45] in the BNNT. The CNT atom composition is only of C (0.70 Å), which defines a homogeneous system[45].

B. Reflected and transmitted probabilities

The angular distribution of reflected and transmitted H atoms can be obtained by calculating the dispersion angle as $\theta = \arccos\left(\vec{v}_i \cdot \vec{v}_f / |\vec{v}_i||\vec{v}_f|\right)$. Here, $\vec{v}_i$ and $\vec{v}_f$ are the associated vectors to the initial and final velocity of reflected or transmitted H atoms, respectively. It is worth noticing that a reflected or transmitted H atom is determined when its final position is larger than 7 Å, as measured from the center of the nanotube, and its velocity vector points outwards from the nanotube.

The angular distribution, as a function of the dispersion angle, is computed as[31]:

$$\frac{dN}{d\Omega} = C \frac{N\left(\theta, \Delta\theta\right)}{2\pi \sin\left(\theta\right) \Delta\theta}, \tag{1}$$

where $N(\theta, \Delta\theta)$ is the number of reflected or transmitted H atoms within the interval $\Delta\theta = 5^o$ and C is a normalization constant. In Fig. 7, we show the angular distribution of the reflected and transmitted H atoms for different impact energies for CNT in a) and BNNT in b). The average of our results over the impact energies for both systems is shown by open triangle symbols in the same figure. We also include a fitting curve to the average of our results. This fitting curve is obtained from the modified Yamamura's formula[46,47]

$$\frac{dN(\theta)}{d\Omega} = \frac{dN(0)}{d\Omega} \left[\cos\left(\Theta^A\right)\right]^{-B} \exp\left[C\left\{1 - \frac{1}{\cos\left(\Theta^A\right)}\right\}\right] \tag{2}$$

where $dN(0)/d\Omega$ is a constant and $\Theta = \theta + \phi$ is the scattering angle. The phase-shift ϕ, and constants $dN(0)/d\Omega$, A, B, and C are fitting parameters in this approach. We use

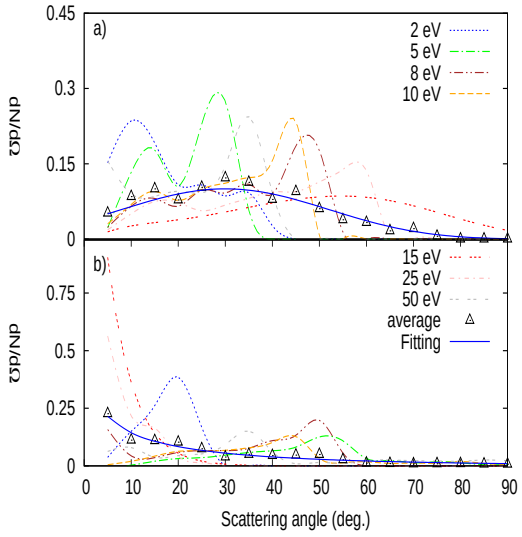

FIG. 7. (Color on-line). Angular distribution of reflected and transmitted H projectiles as a function of the dispersion angle for CNT in a) and for BNNT in b). Open triangle symbols are the average over the impact energies for both systems. We include a fitting curve to modified Yamamura's formula for the average of our results, Eq. (2)

the modified Yamamura's formula since it has been applied to the study of the angular dependence of the sputtering yield in a-C:H surface irradiated by hydrogen[47]. The new fitting curve, used in this work, is obtained from the average of the results in the impact energy range 2-50 eV, where the H impacts are captured and exo-bound. Fitting parameters are listed in Table I for reference purposes. The modified Yamamura's formula fits very well the average with a correlation factor of 0.985 for both cases. We notice that the results for the CNT system follow a $\cos^{7.01}(\theta - 30)$ function. In contrast, the BNNT system results need to be weighted by an exponential function due to the effects of the B and N mixture. At 100 eV, all the H atoms are transmitted and the majority go through the nanotube with no dependence on the direction of the impinging trajectory.

IV. CONCLUDING REMARKS

The atomic hydrogen adsorption and capture by nanotubes is important to understanding the doping and chemical properties of nanotubes with applications in the development of nanosensors. In this work, we perform numerical simulations of atomic hydrogen irradiation on Carbon (CNT) and Boron-nitride (BNNT) nanotubes with a quantum-classical molecular

TABLE I. Fitting parameters for Yamamura formula.

Parameters	BNNT	CNT
$dN(0)/d\Omega$	0.5	0.1
A	0.235	1.0
B	−5.84	−7.01
C	−0.58	0.0
ϕ	0	−30

dynamics based on the SCC-DFTB quantum chemistry approach for a wide impact energy range. Our theoretical method provides a good description of the PEC when compared to the Density Functional Theory approach, which is implemented in the Quantum Espresso scientific software. The effect of atomic hydrogen bombardment on the nanotubes is analyzed by calculating the adsorption and capture rates as a function of the impact energy, as well as the angular distribution of scattered particles. We found that both systems are able to adsorb H atoms at impact energies below 5 eV. The hydrogen atoms are captured by the BNNT in the energy range of 5 to 20 eV with a maximum of 7 % at 10 eV. In contrast, the CNT only captures 5 % between 10 and 50 eV with a peak around 15 eV. For the case of BNNT, the largest capture contribution is due to the B atom since the bonding energy of B-H (3.42 eV) is stronger than the H-N bonding energy (3.2 eV). We also study the role of the carbon system cruvature, i.e., we compare previous results for the scattering of H atoms by fullerene and graphene to our CNT results, finding that for collision energies above 5 eV the scattering process is very similar. However, the curvature plays an important role for low collision energies. Finally, the angular distribution of the reflected and transmitted H atoms follows a modified Yamamura's law. The scattered particles from a CNT follows a cosine distribution while the results for a BNNT target requires an exponential function correction due to the mixture of the boron and nitrogen in this system. Thus, how the H atom is scattered or bound to the CNT or BNNT, modifies the electronic properties of the nanotube, which could serve as a guide for H nanosensor development and to understand the nanotube damage after hydrogen irradiation. As a future work, it is of our interest to analyze the H_2 adsorption mechanism for hydrogenated CNT and BNNT due to the binding of H atoms by boron, leaving the nitrogen atom free to capture upcoming H projectiles in a

multiple H bombarding. This is a work in progress.

ACKNOWLEDGEMENTS

We acknowledge support from A. von Humboldt Foundation for research fellowship to FJDG, as well as to ICF-UNAM for a visiting stay. RCT acknowledges support from DGAPA-UNAM PAPIIT-IN-106-617 and LANCAD-UNAM-DGTIC-228. CMF would like to thank CONACyT scholarship with CVU 424130. Results in this paper were obtained using the LI-red institutional cluster at the Institute for Advanced Computational Science at Stony Brook University and the Comet cluster of the San Diego super computer center which is part of XSEDE.

REFERENCES

[1]P. A. Mildred S. Dresselhaus, Gene Dresselhaus, ed., *Carbon Nanotubes: Synthesis, Structure, Properties, and Applications*, Topics in Applied Physics, Vol. 80 (Springer-Verlag Berlin Heidelberg, 2001).

[2]A. V. Eletskii, Physics-Uspekhi **47**, 1119 (2004).

[3]K. F. Akhmadishina, I. I. Bobrinetskii, I. A. Komarov, A. M. Malovichko, V. K. Nevolin, V. A. Petukhov, A. V. Golovin, and A. O. Zalevskii, Nanotechnologies in Russia **8**, 721 (2013).

[4]A. M. Marconnet, M. A. Panzer, and K. E. Goodson, Rev. Mod. Phys. **85**, 1295 (2013).

[5]H. Reardon, J. M. Hanlon, R. W. Hughes, A. Godula-Jopek, T. K. Mandal, and D. H. Gregory, Energy Environ. Sci. **5**, 5951 (2012).

[6]D. Golberg, Y. Bando, Y. Huang, T. Terao, M. Mitome, C. Tang, and C. Zhi, ACS Nano **4**, 2979 (2010).

[7]R. Orináková and A. Orinák, Fuel **90**, 3123 (2011).

[8]C. Liu, Y. Chen, C.-Z. Wu, S.-T. Xu, and H.-M. Cheng, Carbon **48**, 452 (2010).

[9]X. Wu, J. Yang, J. G. Hou, and Q. Zhu, The Journal of Chemical Physics **121**, 8481 (2004), https://aip.scitation.org/doi/pdf/10.1063/1.1799958.

[10]R. J. Baierle, P. Piquini, T. M. Schmidt, and A. Fazzio, The Journal of Physical Chemistry B **110**, 21184 (2006), pMID: 17048943,

https://doi.org/10.1021/jp061587s.

[11]T. Hübert, L. Boon-Brett, G. Black, and U. Banach, Sens. actuators B **157**, 329 (2011).

[12]I. Sayago, E. Terrado, M. Aleixandre, M. Horrillo, *et al.*, Sens. actuators B **122**, 75 (2007).

[13]M. Xiao, S. Liang, J. Han, D. Zhong, J. Liu, Z. Zhang, and L. Peng, ACS Sensors **3**, 749 (2018), pMID: 29620873, https://doi.org/10.1021/acssensors.8b00006.

[14]J. Suehiro, S. Yamane, and K. Imasaka, in *SENSORS, 2007 IEEE* (2007) pp. 554–557.

[15]A. Oberlin, M. Endo, and T. Koyama, Journal of Crystal Growth **32**, 335 (1976).

[16]N. Arora and N. Sharma, Diamond and Related Materials **50**, 135 (2014).

[17]M. JoseYacaman, M. MikiYoshida, L. Rendon, and J. G. Santiesteban, Applied Physics Letters **62**, 657 (1993).

[18]N. G. Chopra, R. J. Luyken, K. Cherrey, V. H. Crespi, M. L. Cohen, S. G. Louie, and A. Zettl, Science **269**, 966 (1995).

[19]S. Kalay, Z. Yilmaz, O. Sen, M. Emanet, E. Kazanc, and M. Culha, Beilstein J. Nanotechnol. **6**, 84 (2015).

[20]A. Rubio, J. L. Corkill, and M. L. Cohen, Phys. Rev. B **49**, 5081 (1994).

[21]J. Kong, N. R. Franklin, C. W. Zhou, M. G. Chapline, S. Peng, K. J. Cho, and H. J. Dai, Science **287**, 622 (2000).

[22]M. Solimannejad and M. Noormohammadbeigi, Journal of the Iranian Chemical Society **14**, 471 (2017).

[23]C. Wang and C. Guo, Superlattices and microstructures **107**, 97 (2017).

[24]Z. Zhou, J. Zhao, Z. Chen, X. Gao, T. Yan, B. Wen, and P. v. R. Schleyer, The Journal of Physical Chemistry B **110**, 13363 (2006).

[25]M. Elstner, D. Porezag, G. Jungnickel, J. Elsner, M. Haugk, T. Frauenheim, S. Suhai, and G. Seifert, Phys. Rev. B **58**, 7260 (1998).

[26]B. Lukose, A. Kuc, J. Frenzel, and T. Heine, Beilstein J. Nanotechnology **1**, 60 (2010).

[27]J. C. Slater and G. F. Koster, Phys. Rev. **94**, 1498 (1954).

[28]http://www.dftb-plus.info/ (2017).

[29]L. Han and P. Krsti, Nanotechnology **28**, 07LT01 (2017).

[30]C. Ehemann, P. S. Krstic, J. Dadras, P. R. C. Kent, and J. Jakowski, Nanoscale. Res. Lett. **7**, 198 (2012).

[31]M. Novotny, F. J. Dominguez-Gutierrez, and P. Krstic, J. Mater. Chem. C **5**, 5426 (2017).

[32]F. J. Dominguez-Gutierrez, P. S. Krstic, S. Irle, and R. Cabrera-Trujillo, Carbon **134**, 189 (2018).

[33]L. Zhechkov, T. Heine, S. Patchkovskii, G. Seifert, and H. A. Duarte, Journal of Chemical Theory and Computation **1**, 841 (2005).

[34]A. K. Rappe, C. J. Casewit, K. S. Colwell, W. A. Goddard III, and W. M. Skiff, J. Am. Chem. Soc. **114**, 10024 (1992).

[35]T. Hayashi, Y. A. Kim, T. Matoba, M. Esaka, *et al.*, Nano Letters **3**, 887 (2003), https://doi.org/10.1021/nl034080r.

[36]L. F. Sun, S. S. Xie, W. Liu, W. Y. Zhou, Z. Q. Liu, d. S. Tang, G. Wang, and L. X. Qian, Nature **403**, 384 (2000).

[37]C. Q. Sun, H. L. Bai, B. K. Tay, S. Li, and E. Y. Jiang, The Journal of Physical Chemistry B **107**, 7544 (2003), https://doi.org/10.1021/jp035070h.

[38]P. Giannozzi, S. Baroni, N. Bonini, M. Calandra, R. Car, C. Cavazzoni, *et al.*, Journal of Physics: Condensed Matter **21**, 395502 (2009).

[39]J. P. Perdew, K. Burke, and M. Ernzerhof, Phys. Rev. Lett. **77**, 3865 (1996).

[40]P. E. Blöchl, Phys. Rev. B **50**, 17953 (1994).

[41]H. J. Monkhorst and J. D. Pack, Phys. Rev. B **13**, 5188 (1976).

[42]S. Ebrahimi-Nejad and A. Shokuhfar, Physica E: Low-dimensional Systems and Nanostructures **50**, 29 (

[43]A. Geim and K. Novoselov, Nature materials **6**, 183 (2007).

[44]G. E. Froudakis, Materials Today **14**, 324 (2011).

[45]J. C. Slater, The Journal of Chemical Physics **41**, 3199 (1964).

[46]Y. Yamamura, Y. Itikawa, and N. Itoh, IPPJ-AM **26**, 1 (1983).

[47]W. Eckstein and R. Preuss, J. Nucl. Materials **320**, 209 (2003).